PROCEEDINGS OF SCIENCE

Update on the nucleon quark distribution functions calculation with a confining NJL model adding pseudoscalar and vector diquarks

Bailing Ma* **and Ian Cloët**

Argonne National Laboratory,
Lemont, Illinois 60439, USA

E-mail: mab@anl.gov, icloet@anl.gov

We investigate the quark spin-independent and spin-dependent distributions in the nucleon within the framework of a covariant and confining Nambu-Jona-Lasinio (NJL) model. The nucleon bound state is obtained by solving the Faddeev equation in the quark–diquark approximation. In contrast to earlier works, we include not only the scalar and axial vector diquark channels, but now also the pseudoscalar and vector diquarks. The inclusion of these new diquark channels is crucial in maintaining chiral symmetry. Since the scalar and axial vector diquarks have positive parity, they can be in an s-wave state when combined with a quark to form a nucleon, whereas pseudoscalar and vector diquarks have negative parity and so must be in a p-wave state. By including these p-wave diquark correlations, we seek to understand how they affect the quark helicity distributions. We present our calculations for the unpolarized and polarized quark light-front momentum distribution functions and compare them to the available empirical fits. We find the inclusion of these new diquark channels improved the agreement of our model with the empirically-parametrized distribution functions. We obtain the nucleon axial coupling g_A from our calculation as $g_A = 1.42$ for our full model, while $g_A = 1.51$ if we include scalar and axial vector diquarks only. We do not find improvement on the spin sum from adding the pseudoscalar and vector diquarks.

25th International Spin Physics Symposium (SPIN 2023)
24-29 September 2023
Durham, NC, USA

*Speaker

PoS(SPIN2023)186

1. Introduction

In the late 1980s, the European Muon Collaboration (EMC) [1] discovered that only a small fraction of the proton spin is accounted for by the quark spins, triggering the so-called "proton spin crisis" which is still of much interest to the nuclear and particle physics communities today. A complete picture of the proton spin structure requires understanding of the non-perturbative regime of quantum chromodynamics (QCD) which is still missing, except for numerical lattice simulations. More recently, it has been estimated that $\sim 30\%$ of the nucleon spin is carried by the quark spin. The remainder of the spin must arise from the gluon spin and the quark and gluon orbital angular momentum (OAM), and certain sum rules have been derived in regard to their contributions [2]. The gauge-invariant decomposition of the nucleon spin into quark and gluon contributions allows for their measurement in experiments such as deeply virtual Compton scattering (DVCS), and necessitates the study of parton distributions beyond the longitudinal dimension.

In this work, we calculate the spin-independent and spin-dependent quark light-front momentum distribution functions in the framework of a confining NJL model [3–5], which was developed by W. Bentz, A. W. Thomas, and others. A proper-time regularization scheme is introduced to simulate confinement in the absence of gluons, in which an infrared cutoff is applied to eliminate free quark propagation. This model is attractive because it is manifestly covariant and exhibits spontaneous chiral symmetry breaking. It has been used to calculate parton distribution functions (PDFs) [6], nucleon elastic form factors [7], transverse momentum dependent distributions (TMDs) [8], and generalized parton distributions (GPDs) [9, 10]. It has also been used to study medium modifications to the nucleon structure functions in nuclei and nuclear matter [11, 12]. The nucleon in this model is approximated by a bound state of a quark and a diquark [5], in which the diquark is a qq bound state solution to the Bethe-Salpeter equation. We include all the diquark channels of scalar, pseudoscalar, axial vector and vector in this work. We pay special attention to the helicity distributions of the quarks inside a nucleon, especially how the new inclusion of the OAM-carrying diquarks, namely the pseudoscalar and vector diquarks, affect the helicity PDF results, as compared to the truncated model [6], where only scalar and axial vector diquark channels are included.

2. NJL model

The NJL model is a low-energy, effective theory of the strong interaction that mimics many key features of QCD. However, unlike QCD, the NJL model considers only the quarks as the explicit degrees of freedom, neglecting the gluons that are present in QCD. The nucleon is modeled by a relativistic quark-diquark bound state satisfying the Faddeev equation. In the qq channel, the NJL Lagrangian for $SU(2)$ flavor is given by:

$$\begin{aligned}\mathcal{L} = \bar{q}(i\partial\!\!\!/ - \hat{m})q + G_s\left(\bar{q}\gamma_5 C\tau_2\beta_A\bar{q}^T\right)\left(q^T C^{-1}\gamma_5\tau_2\beta_A q\right) - G_p\left(\bar{q}C\tau_2\beta_A\bar{q}^T\right)\left(q^T C^{-1}\tau_2\beta_A q\right) \\ + G_a\left[\left(\bar{q}\gamma_\mu C\vec{\tau}\tau_2\beta_A\bar{q}^T\right)\left(q^T C^{-1}\gamma^\mu\tau_2\vec{\tau}\beta_A q\right) + \left(\bar{q}\gamma_\mu\gamma_5 C\tau_2\beta_A\bar{q}^T\right)\left(q^T C^{-1}\gamma^\mu\gamma_5\tau_2\beta_A q\right)\right],\end{aligned} \tag{1}$$

where $C = i\gamma_2\gamma_0$ is the charge conjugation matrix and $\beta_A = \sqrt{\frac{3}{2}}\lambda_A$ $(A = 2, 5, 7)$ [7]. q is the quark field, $\hat{m} \equiv \mathrm{diag}[m_u, m_d]$ is the current quark mass matrix, which we take as $m_u = m_d$. $\vec{\tau}$ are the Pauli matrices for the $SU(2)$ flavor, and G_s, G_p, and G_a are the coupling constant of the four-fermi interaction in each diquark interaction channel. We will respect the three-flavor chiral symmetry and thus take $G_p = G_s$. From the Lagrangian we can see, without the pseudoscalar and vector diquarks, chiral symmetry is not satisfied. Thus, it is not only interesting but also necessary to include them.

The interaction Lagrangian can be Fierz-symmetrized, so that only direct terms need to be considered after a redefinition of the 4-fermion couplings. One of the interesting feature of this model is the dynamical chiral symmetry breaking (DCSB). By solving the mass gap equation, one obtains a constituent quark mass M which is different from the bare quark mass m, $M > m$ for coupling strengths $G > G_{critical}$, so that $M > 0$, even in the chiral limit $m = 0$. The parameter M is fixed *a priori* in our model to be $M = 400$ MeV.

Then, by solving the corresponding Bethe-Salpeter equations , the coupling strength parameters for different qq channels are related to the diquark mass parameters. Each of the Bethe-Salpeter vertex normalization factors are also determined.

In a covariant formulation, near a bound-state pole, the two-body t matrix behaves as

$$\mathcal{T}(q) \to \frac{\Gamma_i(q)\bar{\Gamma}_i(q)}{q^2 - M_i^2}, \tag{2}$$

where Γ_i is the normalized homogeneous Bethe-Salpeter vertex function for the state i, and $\bar{\Gamma}_i$ is the normalized conjugate vertex. Expanding the denominators about the pole masses,

$$\Pi(q^2) = \Pi(M_i^2) + (q^2 - M_i^2)\frac{\partial}{\partial q^2}\,\Pi(q^2)\Big|_{q^2=M_i^2} + \ldots \tag{3}$$

we find for the diquarks

$$\begin{aligned}
\tau_s(q) &\longrightarrow 4iG_s - \frac{iZ_s}{q^2 - M_s^2 + i\varepsilon}, \\
\tau_a^{\mu\nu}(q) &\longrightarrow 4iG_a g^{\mu\nu} - \frac{iZ_a}{q^2 - M_a^2 + i\varepsilon}\left(g^{\mu\nu} - \frac{q^\mu q^\nu}{M_a^2}\right), \\
\tau_p(q) &\longrightarrow -4iG_p + \frac{iZ_p}{q^2 - M_p^2 + i\varepsilon}, \\
\tau_v^{\mu\nu}(q) &\longrightarrow 4iG_a g^{\mu\nu} - \frac{iZ_v}{q^2 - M_v^2 + i\varepsilon}\left(g^{\mu\nu} - \frac{q^\mu q^\nu}{M_v^2}\right).
\end{aligned} \tag{4}$$

The Bethe-Salpeter vertex normalization factors Z_i are defined so that they are always positive

$$Z_s^{-1} = -\frac{1}{2}\frac{\partial}{\partial q^2}\,\Pi_{PP}(q^2)\Big|_{q^2=M_s^2}, \tag{5}$$

$$Z_a^{-1} = -\frac{1}{2}\frac{\partial}{\partial q^2}\,\Pi_{VV}(q^2)\Big|_{q^2=M_a^2}, \tag{6}$$

$$Z_p^{-1} = \frac{1}{2}\frac{\partial}{\partial q^2}\,\Pi_{SS}(q^2)\Big|_{q^2=M_p^2}, \tag{7}$$

$$Z_v^{-1} = -\frac{1}{2}\frac{\partial}{\partial q^2}\,\Pi_{AA}^{(T)}(q^2)\Big|_{q^2=M_v^2}. \tag{8}$$

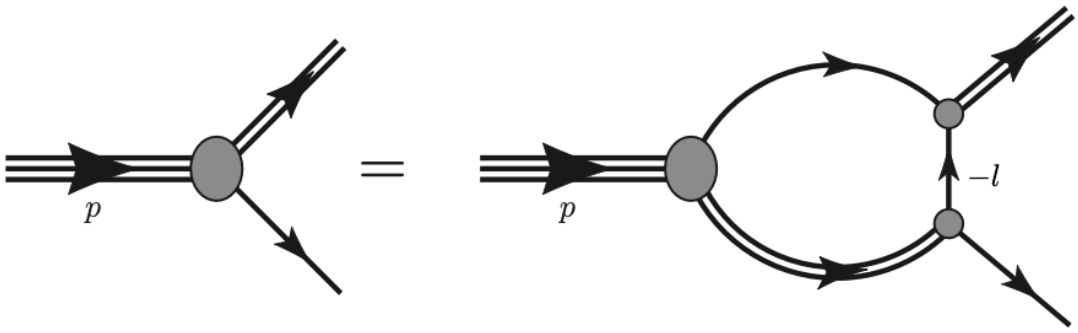

Figure 1: Homogeneous Faddeev equation for the nucleon in the NJL model. The single lines represent the quark propagator and the double lines the diquark propagators. The pseudoscalar and vector diquarks are included in this work in addition to scalar and axial-vector diquarks.

The nucleon is modeled by a relativistic quark-diquark state and satisfies the following Faddeev equation (Fig. 1)

$$\Gamma_N(p,s) = K(p)\,\Gamma_N(p,s), \tag{9}$$

where the kernel is $K \equiv Z\Pi_N$, in which Z is the quark exchange kernel, and Π_N is the quark-diquark bubble matrix. Γ_N is the nucleon vertex function and takes the following form

$$\Gamma_N = \sqrt{-Z_N}\begin{bmatrix} \alpha_1 \\ \alpha_2 \frac{p^\mu}{M_N}\gamma_5 + \alpha_3\gamma^\mu\gamma_5 \\ \alpha_4\gamma_5 \\ \alpha_5 \frac{p^\mu}{M_N} + \alpha_6\gamma^\mu \end{bmatrix} u(p,s), \tag{10}$$

where M_N is the nucleon mass, and the nucleon spinor is normalized such that $\bar{u}(p,s)u(p,s) = 2M_N$. The quark exchange kernel projected onto the color singlet and isospin one-half, in the static approximation where the exchanged quark propagator $S(l) \to -\frac{1}{M}$ [13], becomes

$$Z_{\alpha\beta} = \frac{3}{M}\begin{pmatrix} 1 & \sqrt{3}\gamma^\sigma\gamma_5 & \gamma_5 & \gamma^\sigma \\ \sqrt{3}\gamma_5\gamma^\mu & -\gamma^\sigma\gamma^\mu & \sqrt{3}\gamma^\mu & -\sqrt{3}\gamma^\sigma\gamma^\mu\gamma_5 \\ \gamma_5 & \sqrt{3}\gamma^\sigma & 1 & \gamma^\sigma\gamma_5 \\ -\gamma^\mu & \sqrt{3}\gamma^\sigma\gamma^\mu\gamma_5 & \gamma^\mu\gamma_5 & -\gamma^\sigma\gamma^\mu \end{pmatrix}_{\alpha\beta}. \tag{11}$$

The quark-diquark bubble is given by

$$\Pi_N = \begin{pmatrix} \Pi_{Ns} & 0 & 0 & 0 \\ 0 & \Pi^{\mu\nu}_{Na} & 0 & 0 \\ 0 & 0 & \Pi_{Np} & 0 \\ 0 & 0 & 0 & \Pi^{\mu\nu}_{Nv} \end{pmatrix}, \tag{12}$$

where

$$\Pi_{Ns,a,p,v}(p) = -i\int \frac{d^4k}{(2\pi)^4}\tau_{s,a,p,v}(p-k)iS(k). \tag{13}$$

As an effective theory, the NJL model is non-renormalizable, thus it needs a regularization prescription in order to be well-defined. We use the proper-time regularization scheme

$$\frac{1}{X} = \frac{1}{(n-1)!}\int_0^\infty d\tau\ \tau^{n-1}e^{-\tau X} \longrightarrow \frac{1}{(n-1)!}\int_{1/\Lambda_{UV}^2}^{1/\Lambda_{IR}^2} d\tau\ \tau^{n-1}e^{-\tau X}, \tag{14}$$

where X represents a product of propagators that have been combined using Feynman parametrization. The ultraviolet cutoff Λ_{UV} is needed to render the theory finite, while Λ_{IR} is introduced to mimic confinement.

By solving the Faddeev equation, the model parameters are fitted to the nucleon and delta masses $M_N = 940$ MeV and $M_\Delta = 1232$ MeV. The infrared regulator and the dressed quark mass are assigned their values *a priori*, $\Lambda_{IR} = 240$ MeV and $M = 400$ MeV. The Λ_{UV} is fixed by the pion decay constant and we obtain $\Lambda_{UV} = 645$ MeV. We obtain $G_s = 7.65$ GeV^{-2} and $G_a = 4.91$ GeV^{-2}. The corresponding diquark masses are $M_s = 0.679$ GeV, $M_p = 0.945$ GeV, $M_a = 0.929$ GeV, and $M_v = 1.099$ GeV. Compared to the previous values obtained without the pseudoscalar and vector diquark channels, $M_s = 0.768$ GeV and $M_a = 0.929$ GeV, the scalar diquark mass became smaller, while the axial vector diquark stayed the same. The axial vector diquark mass does not change because the delta baryon Faddeev equation only concerns the axial vector diquark. The normalization factors are found to be $Z_s = 14.8$, $Z_a = 6.73$, $Z_p = 8.95$, $Z_v = 4.13$, and the coefficients in the nucleon vertex function are $(\alpha_1, \alpha_2, \alpha_3, \alpha_4, \alpha_5, \alpha_6) = (0.324, 0.072, -0.275, 0.027, -0.030, -0.361)$ and the nucleon vertex function normalization factor is $Z_N = 43.5$.

3. Quark distribution functions

The leading twist spin-independent and helicity quark light-cone momentum distributions in the nucleon are defined by Eqs. (15) and (16), respectively.

$$f_q(x) = p_- \int \frac{d\xi^-}{2\pi} e^{ixp^+\xi^-} \langle p,s|\bar{\psi}_q(0)\gamma^+\psi_q(\xi^-)|p,s\rangle_c, \tag{15}$$

$$\Delta f_q(x) = p_- \int \frac{d\xi^-}{2\pi} e^{ixp^+\xi^-} \langle p,s|\bar{\psi}_q(0)\gamma^+\gamma_5\psi_q(\xi^-)|p,s\rangle_c, \tag{16}$$

To determine the quark distributions, Eq. (15) can be expressed in a more convenient form, as shown in Ref. [6].

$$f_q(x) = -i\int \frac{d^4k}{(2\pi)^4}\delta\left(x - \frac{k_-}{p_-}\right)\mathrm{Tr}\left[\gamma^+ M_q(p,k)\right], \tag{17}$$

where $M_q(p,k)$ is the quark two-point function in the bound nucleon. This allows the distribution functions to be associated with a straightforward Feynman diagram calculation in any model that describes the nucleon as a bound state of quarks. The Feynman diagrams considered in this calculation are depicted in Fig. 2.

For the calculation of the spin-dependent PDFs, we use the result

$$u(p,s)\bar{u}(p,s) = \left(\not{p} + M_N\right)\frac{1+\gamma_5\not{s}}{2}, \tag{18}$$

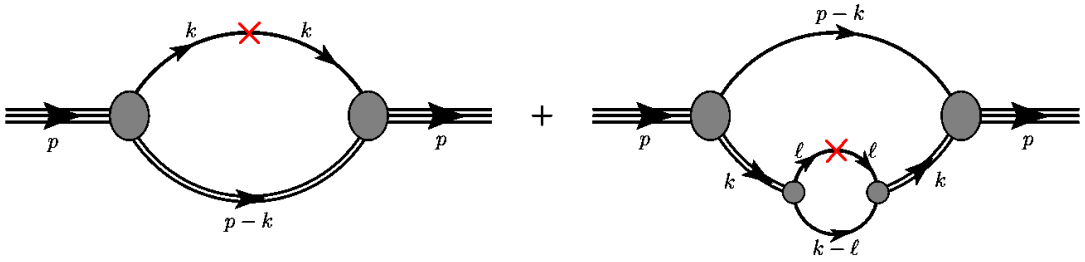

Figure 2: Feynman diagrams representing the quark distributions in the nucleon, needed in the evaluation of Eq. (17). The single line represents the quark propagator and the double line the diquark propagator. The shaded oval denotes the quark-diquark vertex function and the red cross represents the operator insertion which has the form of $\gamma^+\delta(x-k^+/p^+)\frac{1}{2}(1\pm\tau_z)$ for the spin-independent distribution and $\gamma^+\to\gamma^+\gamma_5$ for the spin-dependent one. The left figure where the operator insertion is on the stand alone quark line is referred to as the quark diagram, while the right figure where the operator insertion is on the quark which is within a diquark is called the diquark diagram.

where s^μ is the spin vector of the particle satisfying $s^2=-1$ and $s\cdot p=0$. In general, s^μ can be written as

$$s^\mu=\left(\frac{\vec{p}\cdot\vec{n}}{M_N},\ \vec{n}+\frac{(\vec{p}\cdot\vec{n})\vec{p}}{M_N\left(M_N+p^0\right)}\right) \tag{19}$$

where $\vec{n}=\frac{\vec{p}}{|\vec{p}|}$ if the particle is longitudinally polarized, $\vec{n}\cdot\vec{p}=0$ if transversely polarized.

For the helicity distribution, the proton is longitudinally polarized, and the helicity distribution is defined as

$$\Delta f(x)=f_+(x)-f_-(x), \tag{20}$$

i.e., the difference in the distributions of the quark spin aligned with the proton versus the quark spin anti-aligned with the proton.

In our model, the resulting distributions have no support for negative x, indicating a valence quark picture. By separating the isospin factors, the spin-independent u and d distributions in the proton can be expressed as

$$\begin{aligned}u_v(x)=&f^s_{q/N}(x)+\frac{1}{3}f^a_{q/N}(x)+f^p_{q/N}(x)+f^v_{q/N}(x)+f^{ss}_{q(D)/N}(x)+\frac{5}{3}f^{aa}_{q(D)/N}(x)\\&+f^{pp}_{q(D)/N}(x)+f^{vv}_{q(D)/N}(x)+\frac{2}{\sqrt{3}}f^{pa}_{q(D)/N}(x),\end{aligned} \tag{21}$$

$$d_v(x)=\frac{2}{3}f^a_{q/N}(x)+f^{ss}_{q(D)/N}(x)+\frac{1}{3}f^{aa}_{q(D)/N}(x)+f^{pp}_{q(D)/N}(x)+f^{vv}_{q(D)/N}(x)-\frac{2}{\sqrt{3}}f^{pa}_{q(D)/N}(x). \tag{22}$$

Due to the isospin structures, the scalar, pseudoscalar and vector quark diagrams do not contribute to the d quark's distribution in the proton.

The u and d quarks spin-dependent distributions in the proton end up being

$$\begin{aligned}\Delta u_v(x)=&\Delta f^s_{q/N}(x)+\frac{1}{3}\Delta f^a_{q/N}(x)+\Delta f^p_{q/N}(x)+\Delta f^v_{q/N}(x)+\frac{5}{3}\Delta f^{aa}_{q(D)/N}(x)\\&+\Delta f^{vv}_{q(D)/N}(x)+2\,\Delta f^{sp}_{q(D)/N}(x)+\frac{2}{\sqrt{3}}\Delta f^{sa}_{q(D)/N}(x),\end{aligned} \tag{23}$$

$$\Delta d_v(x) = \frac{2}{3}\Delta f^a_{q/N}(x) + \frac{1}{3}\Delta f^{aa}_{q(D)/N}(x) + \Delta f^{vv}_{q(D)/N}(x) + 2\,\Delta f^{sp}_{q(D)/N}(x) - \frac{2}{\sqrt{3}}\Delta f^{sa}_{q(D)/N}(x). \tag{24}$$

Here, the scalar and pseudoscalar diquark diagrams spin-dependent distributions vanish because of lack of spin structures, however, the scalar-pseudoscalar transition diquark diagram does not vanish because of parity.

Importantly, in this covariant framework, the Ward identities corresponding to number and momentum conservation are satisfied, guaranteeing the validity of the baryon number and momentum sum rules.

$$\int_0^1 dx\, f_{q/P}(x) = N_{q/P}, \quad \int_0^1 dx\, x\left[f_{u/P}(x) + f_{d/P}(x)\right] = 1. \tag{25}$$

The model scale is found to be 0.19 GeV^2, which is slightly higher than the previous 0.16 GeV^2. To compare our results to the experimental data, we evolve the PDFs to a higher energy scale where empirical PDFs are available, namely, 5 GeV^2. We used the program package QCDNUM [14] for this evolution.

4. Results

Fig. 3 shows our calculated spin-independent u quark and d quark light-cone momentum distribution in the proton, in comparison with the JAM22 global fit [15]. We have plotted our PDF results both from a full model calculation and from a truncated model without the pseudoscalar and vector diquarks. The agreement of the model calculation with the JAM empirical PDFs is extremely good, and with the full model the agreement is even better.

In Fig. 4 we present the spin-dependent u and d quark distributions in the proton, and again we compare both our full model and truncated model results with the polarized PDFs from JAM22 [15]. For the full model we obtain a g_A value of 1.420, which is in better agreement to the known value of $g_A = 1.267$ than the model with only scalar and axial vector diquarks, which is $g_A = 1.507$. The discrepancy decreased from 0.240 to 0.153. The first polarized moments we obtained are $\Delta u_v = 1.080$ and $\Delta d_v = -0.341$ in the full model, while for the scalar and axial vector only model they are $\Delta u_v = 1.099$ and $\Delta d_v = -0.408$. The spin sum is 0.739 for the full model which is worse than the 0.691 for the scalar and axial vector only model.

Finally, in Fig. 5, we compare our predicted ratios ($\Delta q/q$) with the JAM22 fit, where the JAM data are only plotted up to $x = 0.85$ and simply filled for $x \in [0.85, 1]$, while the model results are plotted all the way up to $x = 1$. As $x \to 1$, our result calculated from the full model gives $\Delta u/u \approx 0.78$ while $\Delta d/d \approx -0.33$. In comparison, the model with only scalar and axial vector diquarks gives $\Delta u/u \approx 0.80$ while the $\Delta d/d$ ratio approaches -0.17.

5. Conclusion

We used the framework of the relativistic Faddeev equation in the NJL model to calculate the quark light-cone momentum distributions in the nucleon based on a straightforward Feynman diagram evaluation. The work can be extended to calculate GPDs and TMDs or to a finite baryon density calculation.

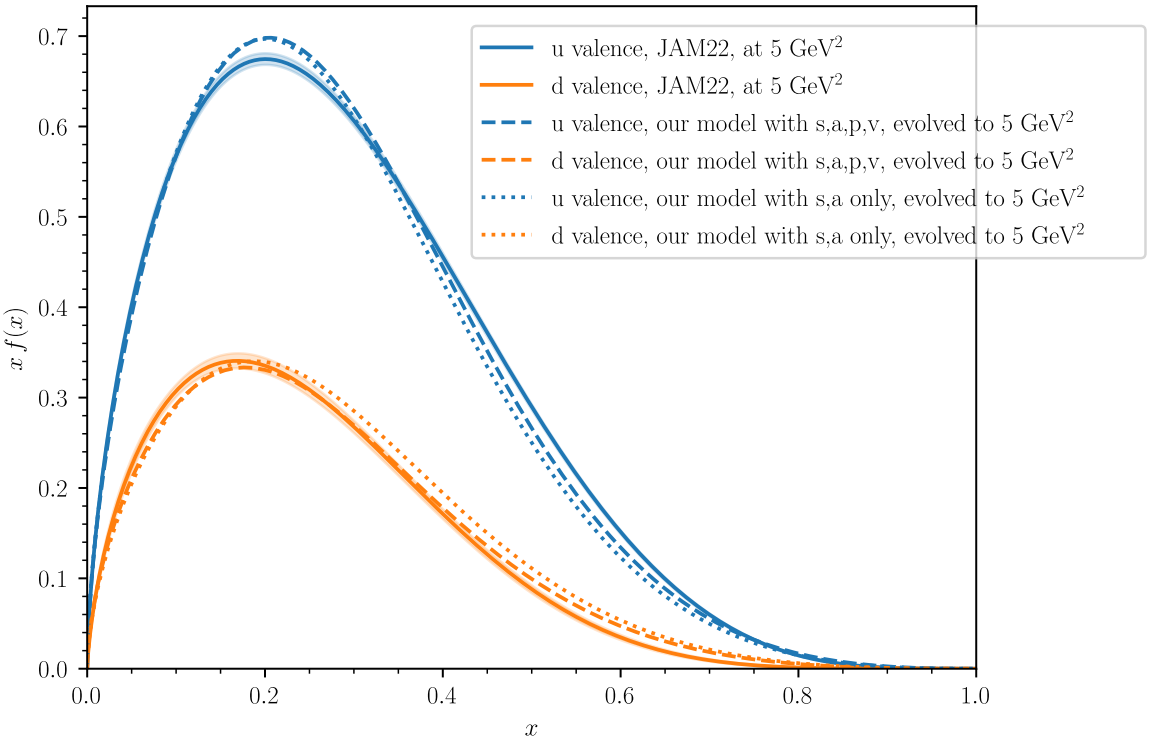

Figure 3: Comparison between our full model and truncated model with the results of JAM22 for the spin-independent PDF. Error bars for JAM22 are at 1σ.

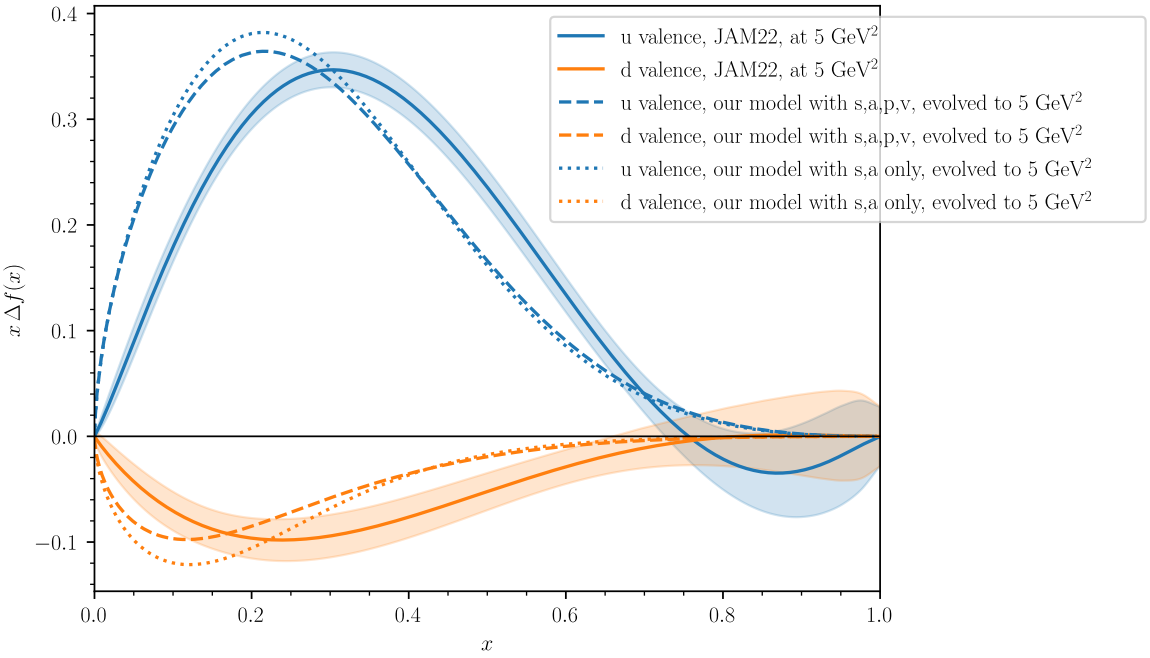

Figure 4: Comparison between our full model and truncated model with the results of JAM22 for the spin-dependent PDF. Error bars for JAM22 are at 1σ.

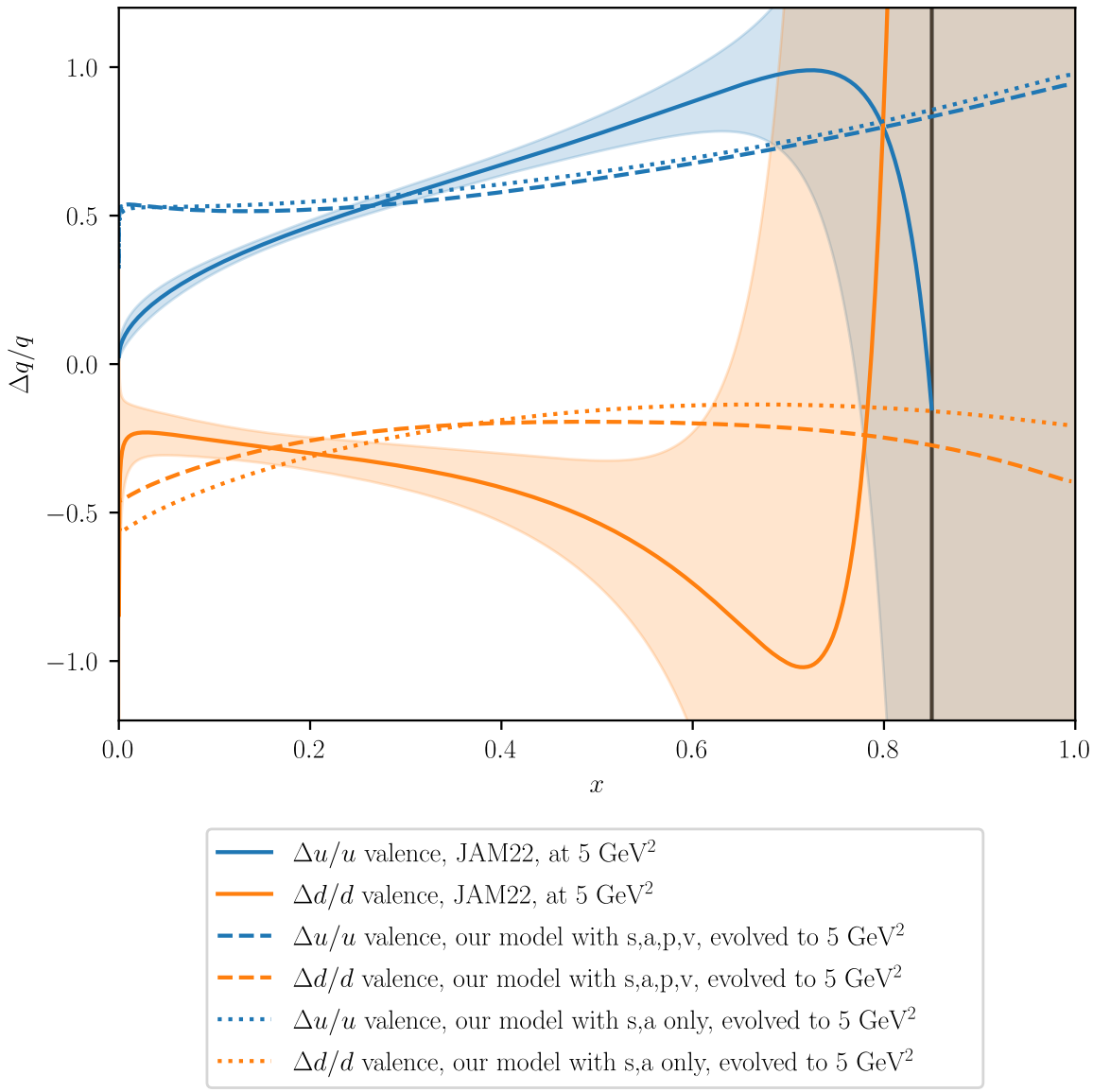

Figure 5: Comparison of $\Delta q/q$ between both our full model and truncated model with the results of JAM22. Error bars for JAM22 are at 1σ. The JAM result are plotted only up to $x = 0.85$ (grey vertical line) while the model calculations are plotted for the full range of $x \in [0, 1]$.

6. Acknowledgements

We gratefully acknowledge the use of the Bebop cluster in the Laboratory Computing Resource Center at Argonne National Laboratory.

References

[1] J. Ashman, et al., European Muon Collaboration, Phys. Lett. **B206** 364, (1988).

[2] Xiang-Dong Ji, Phys. Rev. Lett. **78** 610, (1997).

[3] Y. Nambu and G. Jona-Lasinio, Phys. Rev. **122**, 345 (1961).

[4] Y. Nambu and G. Jona-Lasinio, Phys. Rev. **124**, 246 (1961).

[5] W. Bentz, A.W. Thomas, Nucl. Phys. **A696**, 138 (2001).

[6] I. C. Cloët, W. Bentz, and A. W. Thomas, Phys. Lett. **B621**, 246 (2005).

[7] I. C. Cloët, W. Bentz, and A. W. Thomas, Phys. Rev. **C90**, 045202 (2014).

[8] Y. Ninomiya, W. Bentz, and I. C. Cloët, Phys. Rev. **C96**, 045206 (2017).

[9] A. Freese and I. C. Cloët, Phys. Rev. **C101**, 035203 (2020).

[10] A. Freese and I. C. Cloët, Phys. Rev. **C103**, 045204 (2021).

[11] H. Mineo, W. Bentz, N. Ishii, A. W. Thomas, K. Yazaki, Nucl. Phys. **A735**, 482 (2004).

[12] I. C. Cloët, W. Bentz, and A. W. Thomas, Phys. Lett. **B642**, 210 (2006).

[13] A. Buck, R. Alkofer, and H. Reinhardt, Phys. Lett. **B286**, 29 (1992).

[14] M. Botje, Comput. Phys. Commun. **182**, 490 (2011), arXiv:1005.1481, Erratum arXiv:1602.08383 (2016).

[15] C. Cocuzza, W. Melnitchouk, A. Metz, and N. Sato (Jefferson Lab Angular Momentum (JAM) Collaboration), Phys. Rev. **D106**, L031502 (2022).